

High-Capacity, Dendrite-Free, and Ultrahigh-Rate Lithium-Metal Anodes Based on Monodisperse N-Doped Hollow Carbon Nanospheres

Yuping Liu, Yanzhong Zhen, Taoran Li, Frederik Bettels, Tao He, Manhua Peng, Yucang Liang,* Fei Ding, and Lin Zhang*

To unlock the great potential of lithium metal anodes for high-performance batteries, a number of critical challenges must be addressed. The uncontrolled dendrite growth and volume changes during cycling (especially, at high rates) will lead to short lifespan, low Coulombic efficiency (CE), and security risks of the batteries. Here it is reported that Li metal anodes, employing the monodisperse, lithiophilic, robust, and large-cavity N-doped hollow carbon nanospheres (NHCNSs) as the host, show remarkable performances—high areal capacity (10 mAh cm⁻²), high CE (up to 99.25% over 500 cycles), complete suppression of dendrite growth, dense packing of Li anode, and an extremely smooth electrode surface during repeated Li plating/stripping. In symmetric cells, a highly stable voltage hysteresis over a long cycling life >1200 h is achieved, and a low and stable voltage hysteresis can be realized even at an ultrahigh current density of 64 mA cm⁻². Furthermore, the NHCNSs-based anodes, when paired with a LiFePO₄ (LFP) cathode in full cells, give rise to highly improved rate capability (104 mAh g⁻¹ at 10 C) and cycling stability (91.4% capacity retention for 200 cycles), enabling a promising candidate for the next-generation high energy/power density batteries.

1. Introduction

Li-ion batteries (LIBs) have been widely used in portable electronics and electric vehicles. However, the limited energy/power densities of current LIBs hinder their further applications in high-density energy storage systems.^[1,2] Cathodes with large specific capacity (such as sulfur and oxygen-based cathodes) have made great progress in recent years.^[3] On the anode side, Li metal is considered as the ultimate choice to construct the next-generation battery systems (including Li-S and Li-O₂ batteries), due to its highest specific capacity (3860 mAh g⁻¹), the lowest negative electrochemical potential (-3.04 V vs standard hydrogen electrode) and lightweight.^[2,4]

Li metal was introduced as anode decades ago, but the inevitable Li dendrite growth leads to the security risks and blocked its large-scale commercial applications.^[5] With intensive research efforts in recent years, Li metal anode is now ready


for a revival.^[6] To unlock its great potential, a number of critical issues need to be addressed, for example, the dendrite growth, the large volume change during charge/discharge, as well as the adverse reactions between Li and organic electrolytes. These problems will result in the poor CE, the fast decay of capacity, and even the catastrophic thermal runaway.^[7,8]

Many strategies have been proposed recently to overcome the above-mentioned issues, such as the development of functional liquid electrolytes additives (LiNO₃, LiF, etc.) to form stable solid electrolyte interphase (SEI),^[9] using solid-state electrolytes to avoid the Li dendrites,^[10] and introducing the heteroatom-doped to form lithiophilic surface to guide uniform Li nucleation.^[11] However, these strategies cannot accommodate the huge volume change of Li metal during the repeated charging/discharging, and as a result, the capacity of Li metal anodes drops dramatically. Porous and conductive 3D scaffolds/hosts are expected to accommodate the volume change and allow the uniform deposition of Li metal during charge/discharge,^[12] for example, the works with 3D porous Cu current collectors.^[13] Interconnected carbon nano/microspheres are also an attractive candidate, due to their excellent capability to accommodate the volume changes. The lightweight of these materials

Dr. Y. Liu, T. Li, F. Bettels, T. He, Dr. M. Peng, Prof. F. Ding, Prof. L. Zhang
Institute of Solid State Physics
Leibniz University Hannover
Appelstrasse 2, 30167 Hannover, Germany
E-mail: l.zhang@fkp.uni-hannover.de

Dr. Y. Liu, T. Li, F. Bettels, T. He, Dr. M. Peng, Prof. F. Ding, Prof. L. Zhang
Laboratory of Nano and Quantum Engineering (LNQE)
Leibniz University Hannover
Schneiderberg 39, 30167 Hannover, Germany

Prof. Y. Zhen, Dr. Y. Liang
Institute of Inorganic Chemistry
Eberhard Karls University of Tübingen
Auf der Morgenstelle 18, 72076 Tübingen, Germany
E-mail: yucang.liang@uni-tuebingen.de

 The ORCID identification number(s) for the author(s) of this article can be found under <https://doi.org/10.1002/smll.202004770>.

© 2020 The Authors. Published by Wiley-VCH GmbH. This is an open access article under the terms of the Creative Commons Attribution License, which permits use, distribution and reproduction in any medium, provided the original work is properly cited.

DOI: 10.1002/smll.202004770

can effectively increase the overall energy density of the composite electrodes. However, the Li deposition capacity and current density of the carbon nano/microsphere-based electrodes are fairly low,^[8,14] which is becoming a major challenge for this material system. In order to achieve the target of 500 Wh kg⁻¹ energy density, the Li metal anodes need to be operated with an areal capacity of ≥ 10 mAh cm⁻², a practical current density of ≥ 1 mA cm⁻², and a high Li utilization of $\geq 90\%$.^[15]

In this work, monodisperse, lithiophilic, robust, and large-cavity N-doped hollow carbon nanospheres (NHCNSs) with uniform microstructures were prepared by a microemulsion approach and carbonization (see method). Then, they were coated onto the Cu foil and used as a 3D host for constructing Li metal anodes. We observe that, 1) the lithiophilic nitrogen-containing functional groups (e.g., pyridinic N and graphitic N) of NHCNSs can reduce the local current density, and can regulate the nucleation process of metallic Li electrodeposition as well as the following growth process.^[11,16] The dendrite growth is completely suppressed in this system; 2) the NHCNSs allow the fast electron and ion transportations; 3) the anodes are highly tolerant to the volume changes during repeated Li plating/stripping, due to the hollow cavity inside the carbon nanospheres and the void space between the carbon nanospheres. As a result of these features, the Li@NHCNSs anodes show highly improved performances—a low Li nucleation overpotential, and the dendrite-free morphology, high areal capacity (10 mAh cm⁻²), high CE (up to 99.25% over 500 cycles), dense packing of Li anode, a highly stable voltage hysteresis over a long cycling life of >1200 h, and stable plating/stripping even under ultrahigh current densities

(up to 64 mA cm⁻²). Thanks to the highly efficient Li plating/stripping process, the newly developed anode also shows great potential in a full cell (paired with the LFP cathode), and a highly improved rate capability (104 mAh g⁻¹ at 10 C) and cycling stability (91.4% capacity retention for 200 cycles) can be achieved.

2. Results and Discussion

2.1. Morphology and Structure of the NHCNSs

Monodisperse NHCNSs were prepared by the reaction of 2,4-dihydroxybenzoic acid (DA) and hexamethylenetetramine (HMT) via a microemulsion approach and carbonization process. As shown in **Figure 1a–c**, the SEM images indicate that the NHCNSs have an average particle size of 538 ± 14 nm, and the TEM images reveal a hollow microstructure with a uniform shell thickness of 63 ± 1 nm and an average hollow cavity diameter of 394 ± 11 nm. High-resolution TEM image (Figure 1c, inset) confirms that these carbon spheres are disordered or amorphous. X-ray diffraction (XRD) pattern only shows a broad peak at $2\theta = 43.5^\circ$, which is indexed to the (100) plane for graphite, but no diffraction peak can be observed at $2\theta = 26.5^\circ$ (Figure 1d).

The Raman spectrum of NHCNSs is shown in Figure 1e. The D-band at 1346 cm⁻¹ was observed, which is caused by the defect and disorder-induced modes of disordered or glassy carbon.^[17] The G-band at 1599 cm⁻¹ corresponds to the E_{2g} phonon mode of C sp² atoms from graphite.^[18] The high-intensity ratio ($I_D/I_G = 0.96$) of D band and G band of NHCNSs and the absence

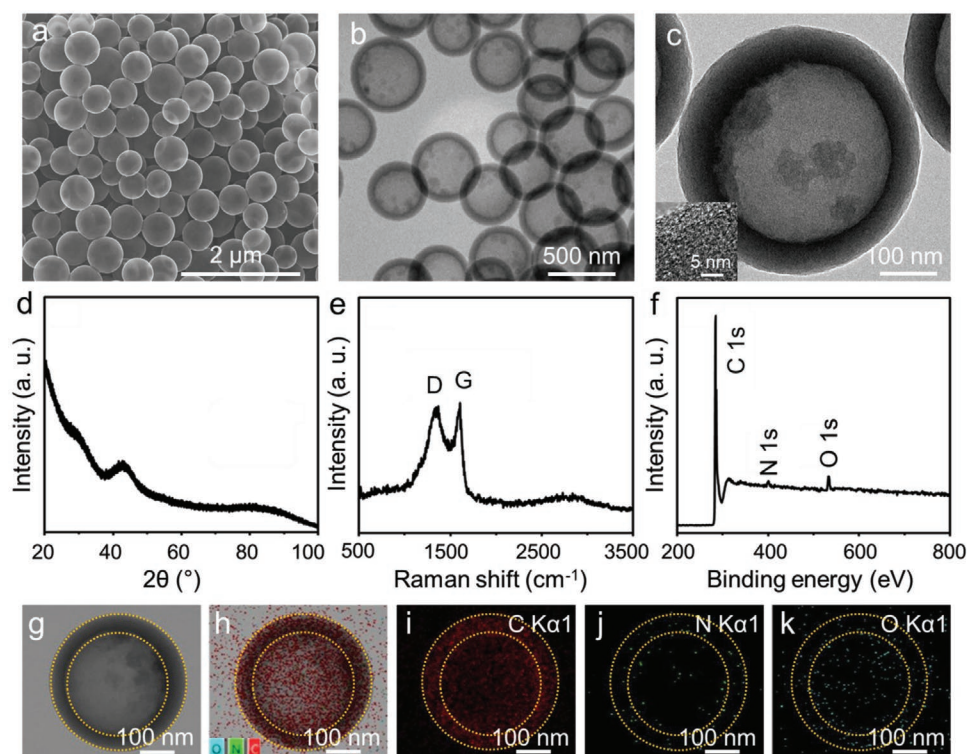


Figure 1. Morphology and structure of the NHCNSs. a) SEM image, b,c) TEM images, d) XRD pattern, e) Raman spectrum, f) survey scanning XPS spectrum, g) single NHCNS, and h) energy-dispersive X-ray spectroscopic elemental mapping, the distribution of elements: i) C, j) N, k) O. The inset shows the HRTEM image in (c). The orange dashed circles in (g)–(h) indicate the shape of a single sphere.

of 2D band at $\approx 2680\text{ cm}^{-1}$ further confirm a high degree of disorder of the NHCNSs, which is in good agreement with the TEM and XRD data. Moreover, X-ray photoelectron spectroscopy (XPS) was performed, which clearly proves the existence of C, N, and O elements (Figure 1f). To further analyze the chemical states of NHCNSs, the energy dispersive X-ray microanalysis and the high-resolution XPS spectra were also performed. X-ray microanalysis confirms the distribution of C, N, and O atoms in NHCNSs and a trace amount of N content derived from the HMT (Figure 1g–k). In the high-resolution XPS spectra of C, N, and O (Figure S1a–c, Supporting Information), the two C 1s peaks correspond to the C=C (284.4 eV) and C–N or C–O (285.4 eV) bonds, the two N 1s peaks are from the electronic states of pyridinic N (398.6 eV) and graphitic N (400.9 eV), and the one O 1s peak is identified as C–OH (532.8 eV). The nitrogen doping can significantly enhance the lithiophilic property of the carbon nanospheres.^[16,19] In addition, the N_2 physisorption of NHCNSs was performed, which shows a typical type I isotherm and corroborates a micropore structure with a specific surface area of $521\text{ m}^2\text{ g}^{-1}$, a single point total pore volume of $0.3\text{ cm}^3\text{ g}^{-1}$ at the relative pressure of 0.99, and a micropore volume of $0.234\text{ cm}^3\text{ g}^{-1}$ (Figure S2, Supporting Information).

2.2. Voltage Profiles of the Li Plating/Stripping Process

To evaluate the electrochemical plating/stripping behavior of NHCNSs (after being coated on the Cu foil, see Figure S3, Supporting Information), CR2032-type coin cells were investigated at different current densities and areal capacities. Planar Cu electrodes were also tested for comparison under the same conditions (Figure 2). Figure 2a,b shows the voltage profiles of

Li plating/stripping into/onto NHCNSs and planar Cu cycled at 1 mA cm^{-2} . Benefiting from the lithiophilic surface functional groups, it can be seen that the voltage polarization of the NHCNSs electrode is much smaller than the planar Cu electrode, and the value of polarization for NHCNSs is only 34 mV while for the planar Cu is 53 mV, indicating a more stable Li electrochemical plating/stripping process. When further cycled at a larger plating capacity (5 or 10 mAh cm^{-2}) and a higher current density (2 mA cm^{-2}) (Figure 2c–f), the NHCNSs electrodes still demonstrate a stable plating/stripping process. And the areal capacity of NHCNSs host can be even up to 20 mAh cm^{-2} (Figure S4, Supporting Information). More interestingly, the NHCNSs host can even exhibit stable electrochemical plating/stripping in the corrosive ester-based electrolyte (Figure S5, Supporting Information). On the other hand, the planar Cu electrodes exhibit large polarizations and random voltages at a plating capacity of larger than 5 mAh cm^{-2} , which can be ascribed to the unstable Li/electrolyte interface and the electrical disconnection as a result of repeated growth of Li dendrites. In addition, a Cu foil coated only with PVDF was also tested and shown in Figure S6a, Supporting Information.

2.3. Coulombic Efficiency

CE is a key parameter to evaluate the sustainability of lithium metal anodes, which is defined as the ratio of the stripped Li from the working electrode versus the plated Li onto the working electrode in each cycle.^[8] Here we investigate the CE under different current densities and areal capacities, for both the NHCNSs electrode and the planar Cu electrode. With 1 mAh cm^{-2} of Li plated and then stripped away at up to 1.0 V for each cycle, the average

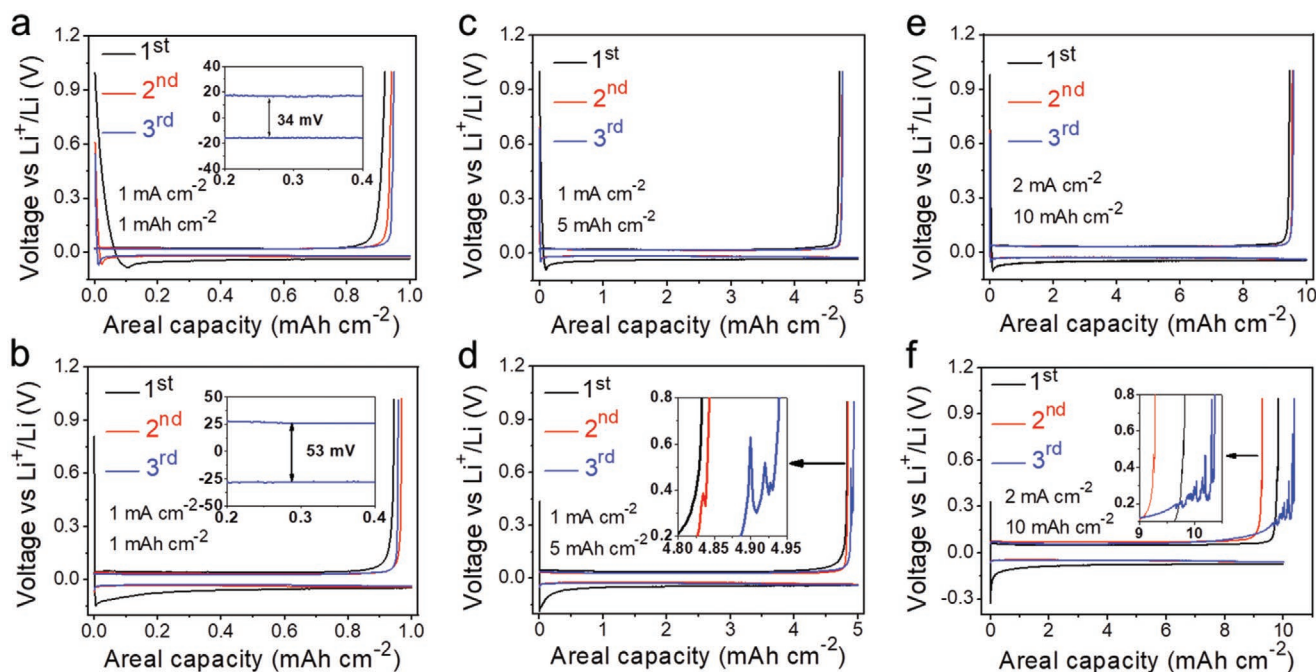


Figure 2. Voltage profiles of the Li plating/stripping process with Li metal as the reference/counter electrode. a) NHCNSs and b) Cu foil with an areal capacity of 1 mAh cm^{-2} at a current density of 1 mA cm^{-2} , c) NHCNSs and d) Cu foil with an areal capacity of 5 mAh cm^{-2} at a current density of 1 mA cm^{-2} , e) NHCNSs and f) Cu foil with an areal capacity of 10 mAh cm^{-2} at a current density of 2 mA cm^{-2} . Insets are enlarged profiles.

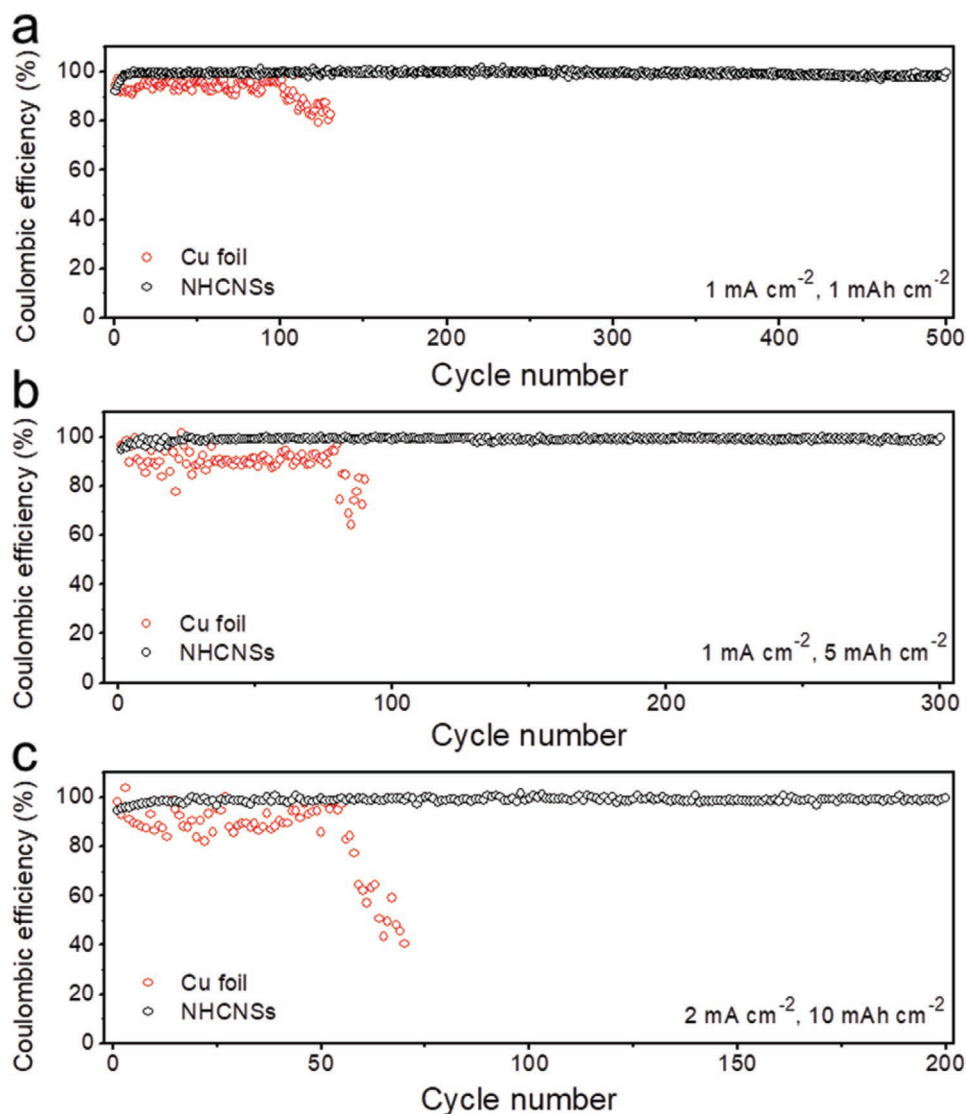


Figure 3. Electrochemical performance—Coulombic efficiency. a) CE of NHCNSs and the Cu foil electrode with an areal capacity of 1 mAh cm^{-2} at a current density of 1 mA cm^{-2} , b) CE of NHCNSs and the Cu foil electrode with an areal capacity of 5 mAh cm^{-2} at a current density of 1 mA cm^{-2} , c) CE of NHCNSs and the Cu foil electrode with an areal capacity of 10 mAh cm^{-2} at a current density of 2 mA cm^{-2} .

CE of NHCNSs electrode was 99.25% for the first 500 cycles at 1 mA cm^{-2} , significantly higher than that of the planar Cu electrode (92.65% for the first 130 cycles) (Figure 3a). Furthermore, the CE exhibited much larger fluctuations for the planar Cu electrode, while it is very stable overall the cycles for the NHCNSs electrode. This is more obvious when the areal capacity was increased to 5 mAh cm^{-2} (Figure 3b). Even with a high areal capacity of 10 mAh cm^{-2} and cycled at 2 mA cm^{-2} , the NHCNSs electrode could still maintain a high average CE of about 98.89% for 200 cycles, while the CE of the planar Cu electrode dramatically dropped to 40% only after 70 cycles and exhibited large fluctuations (Figure 3c). The lower CE of planar Cu electrodes is due to the vulnerable SEI, which is a result of the continuous consumption of newly deposited Li; while the large fluctuation (CE > 100%) can be attributed to the disconnected Li dendrite/mossy from previous cycles.^[20] The higher and stable CE of the

NHCNSs electrodes confirm the uniform deposition of Li, and the formation of a stable SEI that can accommodate the volume change during the repeated plating/stripping processes. The results for the electrodes with PVDF-coated Cu are shown in Figure S6b, Supporting Information.

2.4. Morphology Characterization of the Li Metal Anodes

After repeated plating/stripping, the Li metal morphology was observed under ex-situ SEM. The mechanisms of Li deposition on Cu foil and NHCNSs are illustrated in Figure 4a,b, respectively. During the plating, the NHCNSs were lithiated first, followed by the nucleation of Li metal inside the nanospheres, and then deposit in the cavity of the NHCNSs along with the front Li or the NHCNSs shell until the Li metal filled with part of

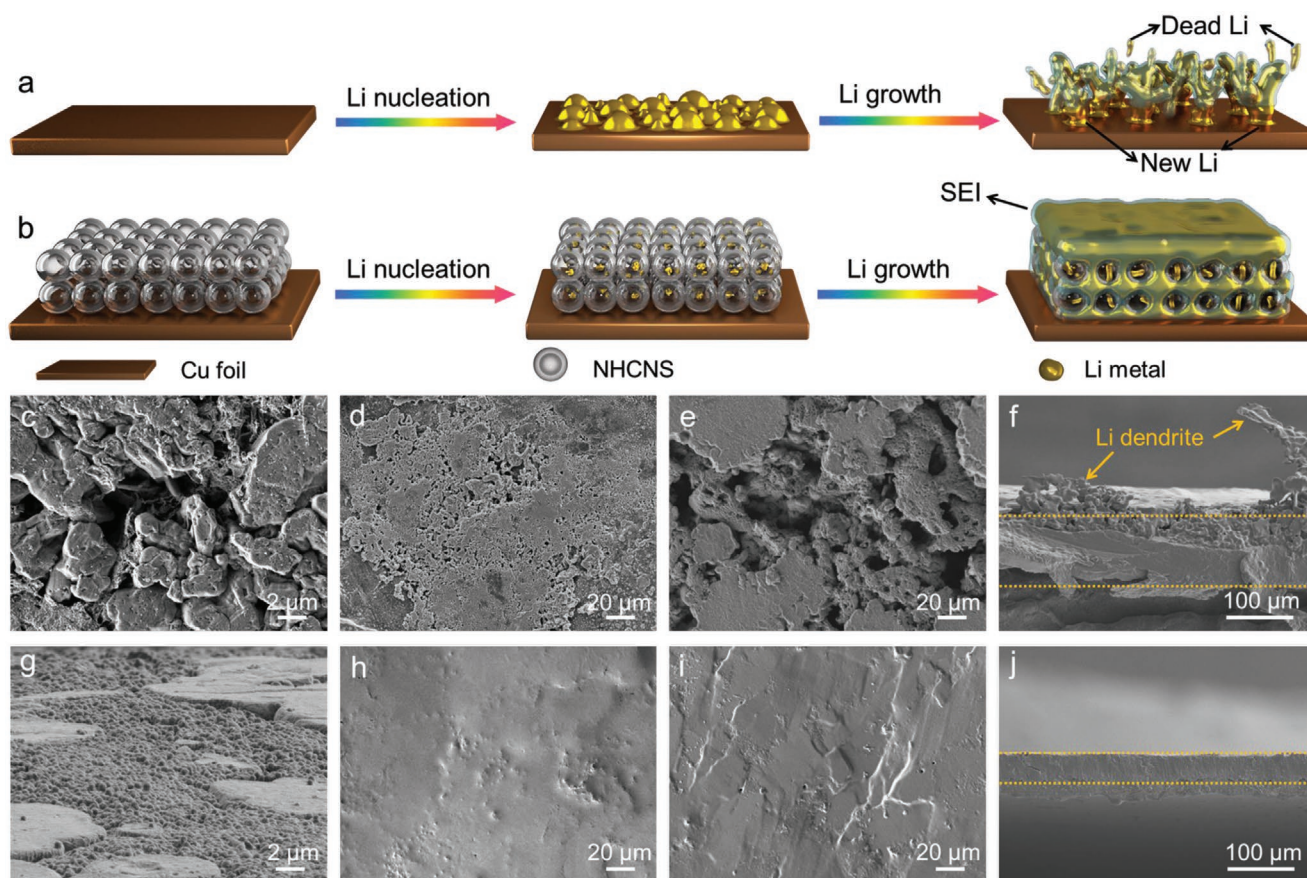


Figure 4. Schematic illustration of Li growth on a) Cu foil and through b) 3D NHCNSs host. Morphology characterization of the Li metal anodes after plating/stripping, top-view SEM images after plating: c) Cu foil and g) NHCNSs with an areal capacity of 1 mAh cm^{-2} at a current density of 1 mA cm^{-2} , d) Cu foil and h) NHCNSs with an areal capacity of 5 mAh cm^{-2} at a current density of 1 mA cm^{-2} , e) Cu foil and i) NHCNSs with an areal capacity of 10 mAh cm^{-2} at a current density of 2 mA cm^{-2} . Cross-sectional SEM images after plating: f) Cu foil and j) NHCNSs with an areal capacity of 10 mAh cm^{-2} at a current density of 2 mA cm^{-2} .

the hollow cavity. As the growth continued, the Li metal filled the void space between the NHCNSs until the entire host was covered.^[21] Due to the uncontrolled Li dendrite growth, which will produce dead Li, exposes new Li, and hence continuously consume the electrolyte, the Li metal anodes typically exhibit a fast capacity decay and a low CE. Here, the NHCNSs host allows a uniform Li deposition and the formation of a stable SEI. Figure 4c–j shows the top/cross-sectional view images of planar Cu and NHCNSs electrodes after five cycles under different areal capacities and current densities. For the planar Cu electrode, even cycled under a relatively low current density of 1 mA cm^{-2} and areal capacity of 1 mAh cm^{-2} , the Li mossy/dendrite growth could be clearly observed (Figure 4c). By further increasing the areal capacities and current densities (Figure 4d,e), more Li moss/dendrites and cracks can be observed for the Cu electrodes. This will increase the Li metal exposure to the organic electrolyte and aggravate adverse reactions, resulting in the fast capacity decay and low CE. These results are consistent with that of the CE (Figure 3). For the NHCNSs electrodes, it is clear to observe that Li was first plated into the hollow cavities (Figure S7, Supporting Information) and the free voids between the carbon nanospheres (Figure 4g). And we can observe that the nanospheres structure

of all the NHCNSs remain intact after the Li deposition, which also illustrates the mechanical robustness of NHCNSs host during the electrochemical process. With more Li plating, the carbon nanospheres were covered by Li but could still achieve an extremely homogeneous Li metal deposition surface morphology (Figure 4h,i). The surface is quite flat, proving that the Li mossy/dendrite growth was successfully suppressed by the carbon nanospheres. This is further corroborated by the cross-section SEM images (10 mAh cm^{-2}) (Figure 4f,j), from which one can also see that the packing density of Li is significantly higher for the NHCNSs electrode. The thickness for the Cu electrode is $\approx 100 \mu\text{m}$, while for the NHCNSs electrode is only $\approx 50 \mu\text{m}$. So the average thickness of the Li@NHCNSs anode per 1 mAh cm^{-2} is $5 \mu\text{m}$, which corresponds to a volume of $5 \times 10^{-4} \text{ cm}^3$ and a mass of $2.6 \times 10^{-4} \text{ g}$. Therefore, the mass/volume ratio is 0.52 g cm^{-3} —very close to the theoretical density of Li metal (0.534 g cm^{-3}). This further demonstrates that Li can be deposited onto the NHCNSs host without porosity (that produced by Li dendrite/moss). This dense packing of Li greatly increases the volumetric energy density of the battery, as we will show later. The cross-sectional SEM images of Li@NHCNSs anodes with 1 mAh cm^{-2} and 5 mAh cm^{-2} areal capacities are shown in Figure S8, Supporting Information, respectively.

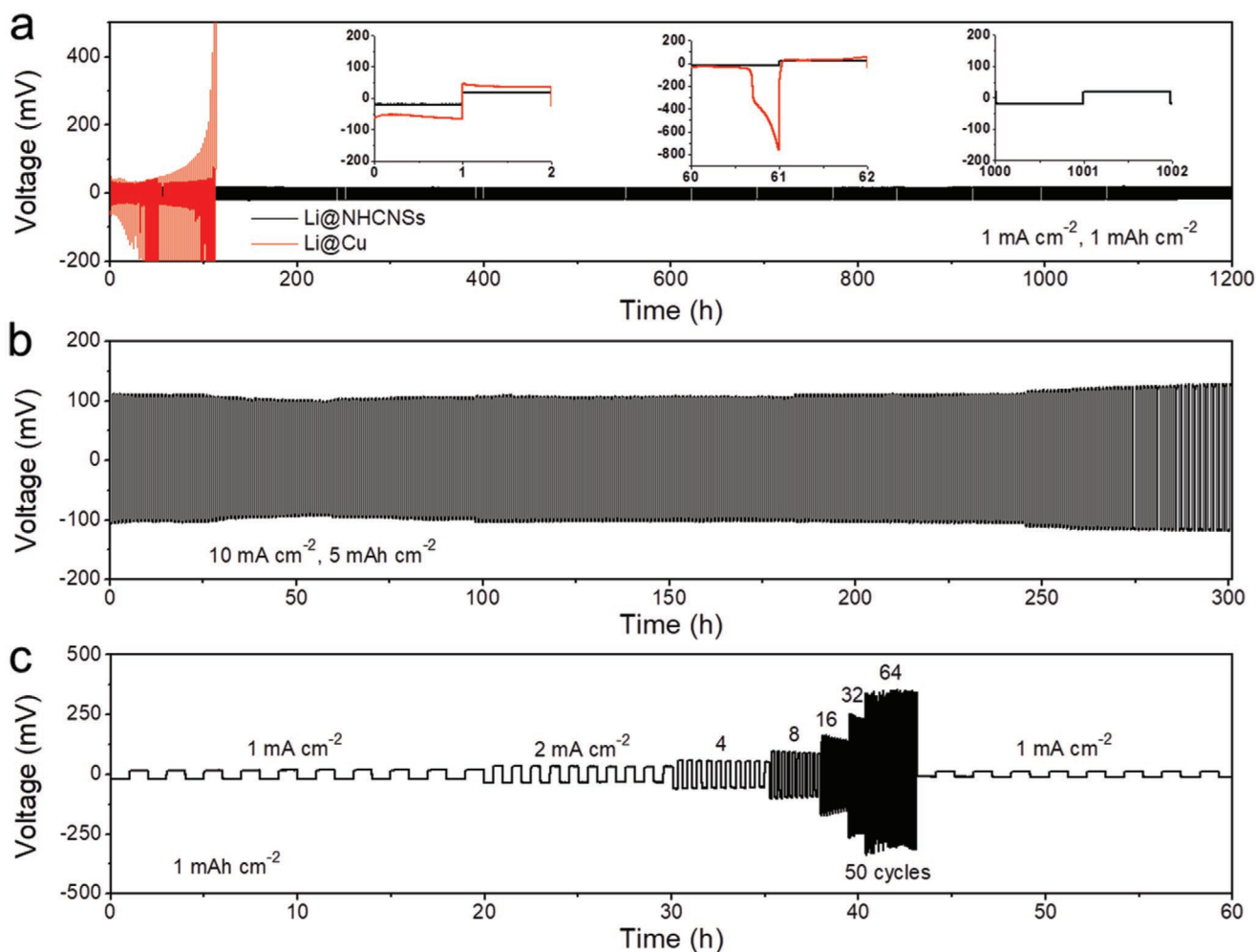


Figure 5. Symmetric cell cycling performances. a) Li@Cu and Li@NHCNSs symmetric cells with a plating/stripping capacity of 1 mAh cm^{-2} at a current density of 1 mA cm^{-2} , b) Li@NHCNSs symmetric cells with a large plating/stripping capacity of 5 mAh cm^{-2} at a large current density of 10 mA cm^{-2} , c) rate performance of Li@NHCNSs electrodes measured at current densities ranging from 1 to 64 mA cm^{-2} at the areal capacity of 1 mAh cm^{-2} . Inset: the detailed voltage profiles at different cycles.

2.5. Symmetric Cell Cycling Performances

To further investigate the electrochemical performances, symmetrical cells were assembled by using the Li@NHCNSs anode ($2 \times$ excess Li was predeposited into/onto the NHCNSs electrode). As a comparison, symmetrical cells based on the Li@Cu anode (predeposited Li onto the planar Cu electrode under the same conditions) were also assembled. **Figure 5a** shows the voltage-time profiles of the symmetric cells with a plating/stripping capacity of 1 mAh cm^{-2} under a current density of 1 mA cm^{-2} . It can be clearly seen that the Li@NHCNSs electrode has a smaller voltage hysteresis ($\approx 17 \text{ mV}$) as well as an outstanding cycling stability for more than 1200 h without appreciable voltage fluctuations. In contrast, the Li@Cu electrode exhibited much-increased overpotential from the initial cycle, which can be ascribed to the unstable Li/electrolyte interface as a result of repeated growth of Li moss/dendrite and hence the continuous consumption of Li metal.^[13] For a detailed comparison, the enlarged voltage profiles of the 1st, 30th, and 500th cycles are shown in the inset of **Figure 5a**.

For the Li@NHCNSs electrode, both the plating and stripping electrochemical processes show a flat voltage plateau and a low voltage hysteresis ($\approx 17 \text{ mV}$), and even after 500 cycles, the voltage profiles still demonstrate a flat voltage plateau. This is among the best performances to date for advanced Li metal anodes.^[22,23] On the other hand, the Li@Cu electrode exhibited a large overpotential with a wavy motion at both the start and the end of each plating/stripping process.

In addition, the voltage hysteresis for Li@NHCNSs cell displays a much smaller value and is stable over 600 cycles (**Figure S9**, Supporting Information). The voltage hysteresis is defined as the difference between the stripping and plating voltage, which is mainly affected by the current density and charge transfer resistance of the cells.^[8,13,22] Due to the unstable interface between Li and electrolyte, the Li@Cu showed a large and irregular fluctuation of voltage hysteresis. In order to understand the greatly reduced voltage hysteresis and the highly stable cycling of Li@NHCNSs electrode, the electrochemical impedance spectra (EIS) was carried out on the symmetric cells before and after cycling (**Figure S10**, Supporting

Information). The Li@NHCNSs electrode exhibited a much lower interfacial charge transfer resistance when compared with the Li@Cu electrode in the symmetric cells. This is an important indication of the faster Li plating/stripping kinetics in the Li@NHCNSs electrode. Also, the Li@NHCNSs electrode resistance showed an even lower value after five cycles (Figure S10a, Supporting Information), which is probably due to the optimization of the interface after several cycles. In contrast, the Li@Cu electrode resistance increased after several cycles (Figure S10b, Supporting Information), owing to the unstable interface of the Li/electrolyte after the growth of moss/dendrite and cracks. These results are consistent with that of the voltage hysteresis analysis (Figure S9, Supporting Information).

To further show the advantages of the Li@NHCNSs anode, the symmetrical cell was tested with a high current density (10 mA cm^{-2}) and a high areal capacity (5 mAh cm^{-2}) (Figure 5b). Stable cycling of over 300 cycles, together with a consistently low overpotential, can be achieved for the Li@NHCNSs electrode. Moreover, the rate capabilities were tested by the symmetric cell cycled at different current densities ranging from 1 to 64 mA cm^{-2} as shown in Figure 5c. The voltage hysteresis was stable during each current density, even at an ultrahigh rate of 64 mA cm^{-2} for 50 cycles. And the symmetrical cell exhibited a long lifetime of >200 cycles even with a larger areal capacity (8 mAh cm^{-2}) at 64 mA cm^{-2} , see Figure S11, Supporting Information. And the corresponding morphology of Li@NHCNSs electrode after cycling is shown in Figure S12, Supporting Information. This performance is superior to that of the most reports on Li-metal anodes, in terms of achievable current densities, voltage hysteresis as well

as stable plating/stripping voltage.^[24] Interestingly, the voltage hysteresis is even smaller than the initial value after when the current density was recovered to 1 mA cm^{-2} , which may due to the formation of a more stable interface after a long cycle. Also, there was no obvious voltage fluctuation when the current density was increased from 1 to 64 mA cm^{-2} (Figure S13, Supporting Information). And the symmetrical cell can also realize stable cycling and long lifespan under ester-based electrolyte (Figure S14, Supporting Information). The excellent rate capability confirms that the high lithiophilic surface area, the large storage space as well as the high conductivity of the NHCNSs can effectively regulate the Li^+ flux and local current densities.

2.6. Electrochemical Performances of the Full Cells

Finally, we investigate the Li@NHCNSs anode by pairing it with the LFP cathode in a full cell. As a control group, the Li@Cu anode was also studied in full cells (Figure 6a; Figure S15, Supporting Information). In general, the Li@NHCNSs||LFP full cell exhibited low polarization and high specific capacity (the specific capacity is based on the mass of LFP cathode, and a mass loading of LFP $\approx 5 \text{ mg cm}^{-2}$), while the Li@Cu||LFP full cell exhibited huge polarization during charge/discharge. This finding is consistent with the studies on the symmetric cell and the EIS. Even compared with a Li foil, the Li@NHCNSs||LFP still demonstrated a lower polarized voltage and a higher capacity (Figure S16, Supporting Information).

The rate capability of the Li@NHCNSs||LFP full cell is significantly better than that of the Li@Cu||LFP full cell, especially

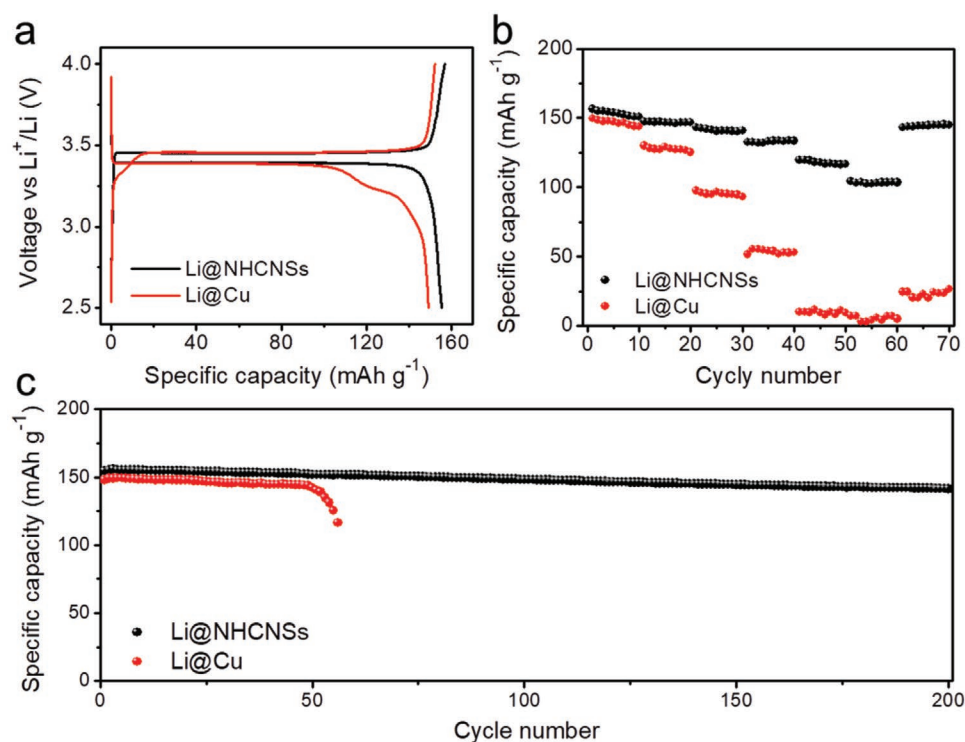


Figure 6. Electrochemical performances of the full cells (LFP as the cathode). a) The charge/discharge profiles cycled at a current density of 0.2 C, b) rate capability cycled at a current density range between 0.2 and 10 C, c) long-term cycling performance cycled at a current density of 0.2 C.

at high current densities. At 10 C, the capacities for the two full cells are 104 and 6 mAh g⁻¹, respectively (Figure 6b). The Li@NHCNSs||LFP full cell also showed an outstanding capacity retention, and exhibited a reversible capacity of 141.4 mAh g⁻¹ after being cycled at a current density of 0.2 C for 200 cycles (about 91.4% capacity retention of the initial capacity of 154.6 mAh g⁻¹). The Li@Cu||LFP full cell, on the other hand, showed a dramatic capacity decay after 45 cycles (Figure 6c), which is mostly due to the fast consumption of Li metal. Moreover, even with only 1.2 × excess Li, the Li@NHCNSs||LFP full cell still displayed relatively large capacity (130 mAh g⁻¹ after 100 cycles). This further confirms that the NHCNSs host can maintain the stable deposition Li metal during the repeated electrochemical process (Figure S17, Supporting Information). With an even higher mass loading (LFP ≈ 10 and 16 mg cm⁻²) and being cycled at a larger current density (1 C), the Li@NHCNSs||LFP full cells can still demonstrate excellent electrochemical performances (Figures S18 and S19, Supporting Information).

3. Conclusions

The interconnected carbon nano/microspheres have a great potential to be used as a host for lithium metal anodes. In this work, monodisperse N-doped hollow carbon nanospheres (NHCNSs) with a uniform size distribution were successfully synthesized by the microemulsion method and then used as a highly efficient host for Li metal anodes. The lithiophilic, robust and large-cavity NHCNSs can completely suppress the Li dendrite growth, allowing an extremely stable Li plating/stripping process at large areal capacities (up to 10 mAh cm⁻²) with dense packing of Li anode, with a relatively low overpotential (≈ 17 mV) and a high CE (up to 99.25% for more than 500 cycles). In the symmetric batteries, the NHCNSs electrodes showed very smooth voltage plateaus even under an ultrahigh rate of 64 mA cm⁻². When paired with LFP cathodes in the full cells, the NHCNSs anodes demonstrated an improved rate capability (104 mAh g⁻¹ at 10 C) and cycling stability (91.4% capacity retention for 200 cycles).

These results compare favorably with that of the recent reports on carbon nano/microsphere-based Li metal anodes (Tables S1–S3, Supporting Information). We believe that the newly developed NHCNSs address the critical issues of uncontrolled dendrite growth and fragile SEI in Li metal anodes and may also be applied to other alkali metal electrodes (e.g., Na and K) for a wide range of applications in advanced batteries.

Supporting Information

Supporting Information is available from the Wiley Online Library or from the author.

Acknowledgements

Y.L. and Y.Z. contributed equally to this work. Y.L. is grateful to Prof. Dr. Reiner Anwander for normal financial support for this research. Y.Z. acknowledges financial support from the China Scholarship Council (CSC).

Open access funding enabled and organized by Projekt DEAL.

Conflict of Interest

The authors declare no conflict of interest.

Keywords

dendrite-free surface, dense Li anode, high capacity, lithium metal anodes, N-doped hollow carbon nanospheres, ultrahigh rate

Received: August 5, 2020

Revised: August 31, 2020

Published online: October 8, 2020

- [1] a) J. M. Tarascon, M. Armand, *Nature* **2001**, *414*, 359; b) M. Armand, J. M. Tarascon, *Nature* **2008**, *451*, 652; c) S. Chu, A. Majumdar, *Nature* **2012**, *488*, 294.
- [2] D. C. Lin, Y. Y. Liu, Y. Cui, *Nat. Nanotechnol.* **2017**, *12*, 194.
- [3] a) H. Wu, Y. Cui, *Nano Today* **2012**, *7*, 414; b) S. Chu, Y. Cui, N. Liu, *Nat. Mater.* **2017**, *16*, 16.
- [4] a) P. G. Bruce, L. J. Hardwick, K. M. Abraham, *MRS Bull.* **2011**, *36*, 506; b) M. D. Tikekar, S. Choudhury, Z. Y. Tu, L. A. Archer, *Nat. Energy* **2016**, *1*, 16114; c) W. Xu, J. L. Wang, F. Ding, X. L. Chen, E. Nasybutin, Y. H. Zhang, J. G. Zhang, *Energy Environ. Sci.* **2014**, *7*, 513; d) Y. Sun, N. Liu, Y. Cui, *Nat. Energy* **2016**, *1*, 16071; e) B. Liu, J. G. Zhang, W. Xu, *Joule* **2018**, *2*, 833; f) X. B. Cheng, R. Zhang, C. Z. Zhao, Q. Zhang, *Chem. Rev.* **2017**, *117*, 10403; g) Y. Liu, S. Ma, L. Liu, J. Koch, M. Rosebrock, T. Li, F. Bettels, T. He, H. Pfnür, N. C. Bigall, A. Feldhoff, F. Ding, L. Zhang, *Adv. Funct. Mater.* **2020**, *30*, 2002462.
- [5] M. S. Whittingham, *Science* **1976**, *192*, 1126.
- [6] a) Y. P. Guo, H. Q. Li, T. Y. Zhai, *Adv. Mater.* **2017**, *29*, 1700007; b) A. Zhamu, G. R. Chen, C. G. Liu, D. Neff, Q. Fang, Z. N. Yu, W. Xiong, Y. B. Wang, X. Q. Wang, B. Z. Jang, *Energy Environ. Sci.* **2012**, *5*, 5701.
- [7] a) Y. Y. Lu, Z. Y. Tu, L. A. Archer, *Nat. Mater.* **2014**, *13*, 961; b) X. B. Cheng, T. Z. Hou, R. Zhang, H. J. Peng, C. Z. Zhao, J. Q. Huang, Q. Zhang, *Adv. Mater.* **2016**, *28*, 2888; c) K. Zhang, G. H. Lee, M. Park, W. J. Li, Y. M. Kang, *Adv. Energy Mater.* **2016**, *6*, 1600811; d) S. Y. Wei, S. Choudhury, Z. Y. Tu, K. H. Zhang, L. A. Archer, *Acc. Chem. Res.* **2018**, *51*, 80.
- [8] G. Y. Zheng, S. W. Lee, Z. Liang, H. W. Lee, K. Yan, H. B. Yao, H. T. Wang, W. Y. Li, S. Chu, Y. Cui, *Nat. Nanotechnol.* **2014**, *9*, 618.
- [9] F. Ding, W. Xu, G. L. Graff, J. Zhang, M. L. Sushko, X. L. Chen, Y. Y. Shao, M. H. Engelhard, Z. M. Nie, J. Xiao, X. J. Liu, P. V. Sushko, J. Liu, J. G. Zhang, *J. Am. Chem. Soc.* **2013**, *135*, 4450.
- [10] H. Duan, Y. X. Yin, Y. Shi, P. F. Wang, X. D. Zhang, C. P. Yang, J. L. Shi, R. Wen, Y. G. Guo, L. J. Wan, *J. Am. Chem. Soc.* **2018**, *140*, 82.
- [11] X. Chen, X. R. Chen, T. Z. Hou, B. Q. Li, X. B. Cheng, R. Zhang, Q. Zhang, *Sci. Adv.* **2019**, *5*, eaau7728.
- [12] a) S. S. Chi, Y. C. Liu, W. L. Song, L. Z. Fan, Q. Zhang, *Adv. Funct. Mater.* **2017**, *27*, 1700348; b) Q. Li, S. P. Zhu, Y. Y. Lu, *Adv. Funct. Mater.* **2017**, *27*, 1606422; c) S. H. Wang, Y. X. Yin, T. T. Zuo, W. Dong, J. Y. Li, J. L. Shi, C. H. Zhang, N. W. Li, C. J. Li, Y. G. Guo, *Adv. Mater.* **2017**, *29*, 1703729; d) S. Jin, Y. Jiang, H. X. Ji, Y. Yu, *Adv. Mater.* **2018**, *30*, 1802014; e) T. T. Zuo, Y. X. Yin, S. H. Wang, P. F. Wang, X. N. Yang, J. Liu, C. P. Yang, Y. G. Guo, *Nano Lett.* **2018**, *18*, 297.
- [13] C. P. Yang, Y. X. Yin, S. F. Zhang, N. W. Li, Y. G. Guo, *Nat. Commun.* **2015**, *6*, 8058.
- [14] a) H. Ye, S. Xin, Y. X. Yin, J. Y. Li, Y. G. Guo, L. J. Wan, *J. Am. Chem. Soc.* **2017**, *139*, 5916; b) Y. G. Lee, S. Ryu, T. Sugimoto, T. Yu, W. S. Chang, Y. Yang, C. Jung, J. Woo, S. G. Kang, H. N. Han,

- S. G. Doo, Y. Hwang, H. Chang, J. M. Lee, J. Y. Sun, *Chem. Mater.* **2017**, *29*, 5906.
- [15] a) H. Kim, G. Jeong, Y. U. Kim, J. H. Kim, C. M. Park, H. J. Sohn, *Chem. Soc. Rev.* **2013**, *42*, 9011; b) S. Jin, Z. W. Sun, Y. L. Guo, Z. K. Qi, C. K. Guo, X. H. Kong, Y. W. Zhu, H. X. Ji, *Adv. Mater.* **2017**, *29*, 1700783; c) C. X. Zu, H. Li, *Energy Environ. Sci.* **2011**, *4*, 2614; d) J. Hassoun, B. Scrosati, *Adv. Mater.* **2010**, *22*, 5198.
- [16] R. Zhang, X. R. Chen, X. Chen, X. B. Cheng, X. Q. Zhang, C. Yan, Q. Zhang, *Angew. Chem., Int. Ed.* **2017**, *56*, 7764.
- [17] T. Jawhari, A. Roig, J. Casado, *Carbon* **1995**, *33*, 1561.
- [18] C. W. Wang, Y. Wang, J. Graser, R. Zhao, F. Gao, M. J. O'Connell, *ACS Nano* **2013**, *7*, 11156.
- [19] D. C. Lin, Y. Y. Liu, Z. Liang, H. W. Lee, J. Sun, H. T. Wang, K. Yan, J. Xie, Y. Cui, *Nat. Nanotechnol.* **2016**, *11*, 626.
- [20] D. Aurbach, E. Zinigrad, Y. Cohen, H. Teller, *Solid State Ionics* **2002**, *148*, 405.
- [21] a) K. Yan, Z. D. Lu, H. W. Lee, F. Xiong, P. C. Hsu, Y. Z. Li, J. Zhao, S. Chu, Y. Cui, *Nat. Energy* **2016**, *1*, 16010; b) W. B. Ye, F. Pei, X. N. Lan, Y. Cheng, X. L. Fang, Q. B. Zhang, N. F. Zheng, D. L. Peng, M. S. Wang, *Adv. Energy Mater.* **2020**, *10*, 1902956.
- [22] K. Yan, H. W. Lee, T. Gao, G. Y. Zheng, H. B. Yao, H. T. Wang, Z. D. Lu, Y. Zhou, Z. Liang, Z. F. Liu, S. Chu, Y. Cui, *Nano Lett.* **2014**, *14*, 6016.
- [23] a) S. F. Liu, X. H. Xia, Y. Zhong, S. J. Deng, Z. J. Yao, L. Y. Zhang, X. B. Cheng, X. L. Wang, Q. Zhang, J. P. Tu, *Adv. Energy Mater.* **2018**, *8*, 1702322; b) M. H. Bai, K. Y. Xie, K. Yuan, K. Zhang, N. Li, C. Shen, Y. Q. Lai, R. Vajtai, P. Ajayan, B. Q. Wei, *Adv. Mater.* **2018**, *30*, 1801213.
- [24] a) G. Huang, J. H. Han, F. Zhang, Z. Q. Wang, H. Kashani, K. Watanabe, M. W. Chen, *Adv. Mater.* **2019**, *31*, 1805334; b) J. Chang, J. Shang, Y. M. Sun, L. K. Ono, D. R. Wang, Z. J. Ma, Q. Y. Huang, D. D. Chen, G. Q. Liu, Y. Cui, Y. B. Qi, Z. J. Zheng, *Nat. Commun.* **2018**, *9*, 4480; c) Z. W. Sun, S. Jin, H. C. Jin, Z. Z. Du, Y. W. Zhu, A. Y. Cao, H. X. Ji, L. J. Wan, *Adv. Mater.* **2018**, *30*, 1800884; d) S. Liu, A. X. Wang, Q. Q. Li, J. S. Wu, K. V. Chiou, J. X. Huang, J. Y. Luo, *Joule* **2018**, *2*, 184.